ICONHIC2026

4th International Conference on Natural Hazards & Infrastructure

29 June – 2 July 2026, Chania, Greece

3DGRIPS: a new rolling/rocking seismic isolation system for lightweight applications

Aristotelis E. Charalampakis, Ph.D.[1]
University of West Attica

George Tsiatas, Ph.D., Panos Tsopelas, Ph.D.
National Technical University of Athens

ABSTRACT

Seismic isolation is a well-established and effective technique for mitigating earthquake-induced damage. However, conventional systems—such as elastomeric bearings, friction bearings, and rolling isolators—exhibit certain limitations, particularly regarding their performance under small vertical loads, challenges related to self-centering, and the management of the vertical component of seismic excitation. The patented 3DGRIPS system is proposed as a solution to these shortcomings and is specifically designed to protect lightweight yet high-value assets, including museum exhibits, servers, and hospital or telecommunications equipment. The isolator incorporates a three-dimensional toothing geometry at its contact surfaces to prevent slippage and enhance damping, combined with a flat resting surface that reduces stress development, provides impact-related damping, and ensures complete recentering to the original equilibrium position after an earthquake. This paper summarizes recent advances within the associated research project, with a focus on data curation efforts and the theoretical analysis of the 3DGRIPS isolator.

Keywords: Rolling isolation system, base isolation, inverse pendulum, museum artefacts

INTRODUCTION

Seismic isolation is an effective method of protection against earthquakes. Instead of increasing the strength of a structure, its purpose is to reduce the seismic forces acting on it. The seismic isolation systems provide (or should provide) the following key components:

(a) The separation of the superstructure from the underlying formation (usually the ground), using flexible elements, which increases the fundamental oscillation period of the system and leads it away from the range of values in which seismic excitations have a strong effect.

(b) The use of damping, in order to keep the displacements within acceptable limits.

(c) The use of some elements of lateral stiffness, which will prevent the significant activation of the system under service loads (as in the case of wind pressure on the superstructure, or weak seismic excitations).

Apart from the common isolation systems which use elastomer or spherical friction bearings, the rolling-type isolation systems are well-known for over 150 years and offer certain advantages. In 1870, J. Touaillon with U.S. Pat. No 99973 patented the seismic isolation system shown in Figure 1. The building is based on rolling metal spheres and therefore there is no significant

[1] Department of Civil Engineering, UNIWA, achar@uniwa.gr, www.charalampakis.com.

acceleration during a seismic event. Similar patents have been awarded to P. Seiler (US846249 – 1907), F. Schär (US951028 – 1910), F.D. Cummings (US1761659 – 1930) and J.F.J. Bakker (US2014643 – 1935). Instead of spheres, cylindrical elements have also been used in one or both dimensions, e.g., the patent awarded to G. C. Lee et al. (US6971795 – 2005).

Rolling isolation systems have the advantage of simplicity but also the significant disadvantage of low damping. Consequently, the displacement requirements are generally excessive. In addition, if the rolling surface is flat, the system does not fully return to its initial position after a dynamic event. This is problematic for the performance of the system in the event of successive seismic excitations. Finally, if the spheres and / or the surfaces on which they roll are made from a soft deformable material such as rubber or polyurethane, to increase damping, the change of shape due to the vertical loads needs attention.

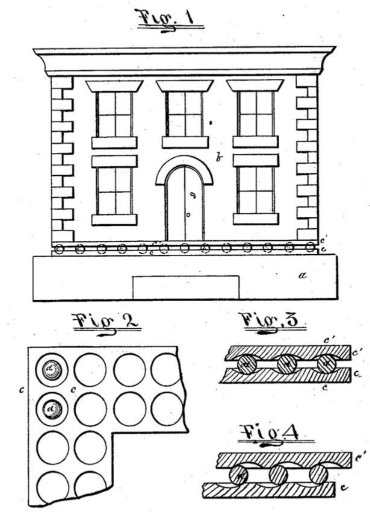

Figure 1. *U.S. Pat. No 99973 by J. Touaillon (1870) (Touaillon, 1870)*

While seismic isolation of newly constructed buildings is common, e.g., the new Stavros Niarchos Foundation Cultural Center in Athens (SNFCC) (Giarlelis et al., 2018), it is generally considered difficult to implement in existing structures. In the latter case, individual seismic protection of the most valuable objects is the most cost-efficient method, e.g., the seismic protection of the statue of Hermes of Praxiteles at the Museum of Olympia (Koumousis V.K., 2008). Apart from museum artefacts, sensitive equipment or whole areas in hospitals, laboratories or data centers can also be seismically protected to ensure their resilience.

Such small-scale applications pose a significant challenge to common seismic isolators due to the following reasons:

(a) Common isolators are not fit for small gravity loads.

(b) Although most seismic isolators exhibit some kind of restoring force, this is weak near the center of the system. Thus, the devices fail to recenter properly and need to be recentered manually. This may not be feasible in time, as it is common for earthquake events to occur in a sequence, one after another, separated by a time span of some minutes or hours. For example, in the recent events in Turkey (6/2/2023), two major earthquakes (Mw 7.8 and Mw 7.5) occurred within 9 hours with an epicentral distance of only 100 km. The subsequent events commence with the system off-center, which may endanger the safety of the objects under protection. As the implementations of seismic isolation grow in number, a system with precise automatic recentering capability is clearly in advantage.

(c) The vertical component of seismic excitation is typically not handled by the common isolation devices, as they only work in the horizontal directions.

To address these shortcomings, a new patented bearing design, called 3-Dimensional Geared Rocking/rolling Inverse Pendulum System (3DGRIPS) (Charalampakis, 2023) is presented herein, which was specifically developed to mitigate these issues.

3DGRIPS

3DGRIPS uses a rocking/rolling inverse pendulum to achieve the separation of the superstructure from its foundation. The defining characteristics which set it apart from other base isolation systems are the following:

(a) The system can be implemented with both a ball-like element (to create a compact bearing of small height, see Figure 2a) or a column element (Figure 2b).

(b) The rolling surfaces in contact feature deep and robust 3D teeth which interlock and ensure that no sliding occurs whatsoever (Figure 3). The depth is sufficient to compensate for potential relative movement in the Z dimension. The engagement of the teeth causes friction and damping, which can be enhanced by proper coating of the involved surfaces with elastomeric or TPU-based materials.

(c) The central part of the bearing is flat which ensures stress alleviation and shape retention, additional impact-related damping, stability under small lateral loads (i.e., no activation under wind loads or small seismic events), and full recentering after a strong dynamic event (see area 5 of Figure 3).

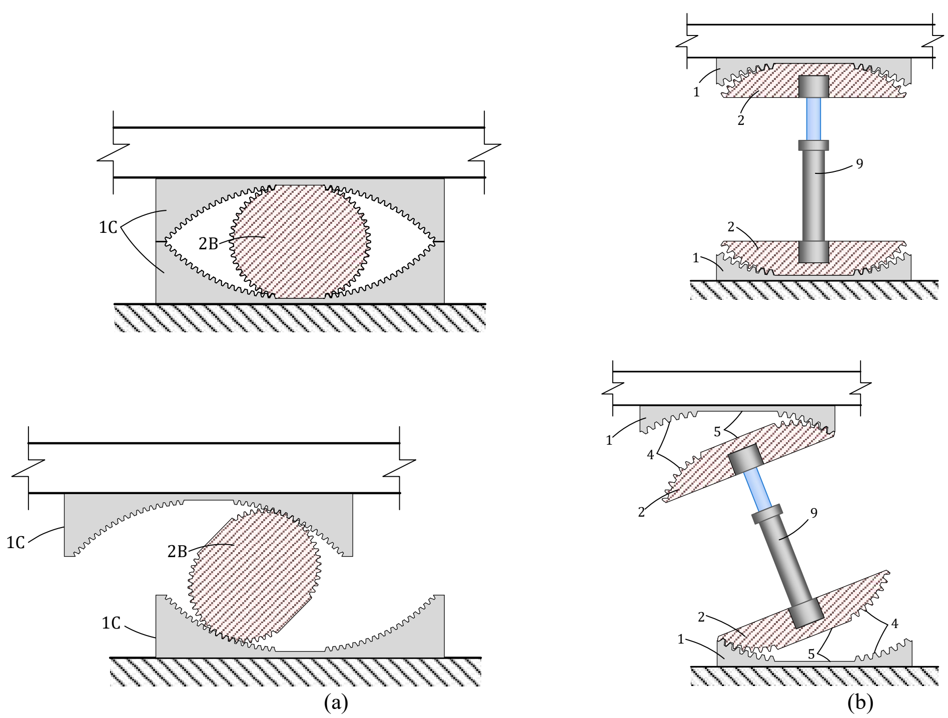

Figure 2. *3DGRIPS (Charalampakis, 2023) with (a) rocking/rolling ball element and (b) rocking/rolling column element with absorber*

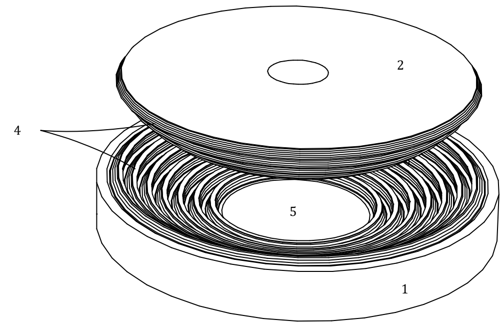

Figure 3. *3D geared contact surfaces of 3DGRIPS (Charalampakis, 2023)*

Contrary to other rolling-type isolators which use deformable TPU balls to increase damping, the present bearing is designed to deform minimally. For this reason, all the kinematic equations can be defined accurately using geometry, and there is no need for complex analyses to account for the deformed shape of the balls and their rolling behavior. The kinematic non-sliding nature of the proposed isolation system also ensures long-term reliability, in contrast to sliding systems where the temporal evolution of the friction coefficient due to aging and contamination should be investigated.

As shown in Figure 2, the deflection of the system from the equilibrium position entails the elevation of the superstructure. Therefore, the gravity loads provide the restoring force, while the curvature of the geared surfaces mainly controls its aggressiveness, just as in spherical friction systems. When the seismic event is over and the bearing is relatively centered, the central flat surfaces act to achieve the completion of the full recentering process. The size of the central flat surface also dictates accurately the threshold, in terms of acceleration, over which the system is activated, just as in rocking systems.

Damping is achieved through the interlocking motion of the gears and the impacts on the central areas. Finally, the displacement capability of the device is similar to a double concave FPS system of equal size.

BEARING DESIGN

The design of the 3DGRIPS bearing allows for various isolator configurations based on the geometry of the central flat areas. No-slip conditions are always assumed, and the gear teeth are omitted from Figure 4 for visual clarity. In all configurations, the orange bases maintain a central flat area identical to that of the corresponding roller. The cases are as follows:

Type-S (Figure 4a): A purely rolling, simple spherical roller with no flat contact surface.

Type-A (Figure 4b): Combines rolling and impact. It is derived by dividing the circular section of a Type-S isolator into two semi-circles, displacing them by $\pm a$ in the horizontal direction, and revolving the resulting ovaloid around the vertical axis of symmetry. The resulting central flat area is a circle of radius a.

Type-B (Figure 4c): Combines rocking/rolling and impact. It is formed by removing horizontal slices from the top and bottom of a full sphere. The central flat area is a circle of radius b.

Type-C (Figure 4d): Combines rocking/rolling and impact. This configuration integrates the design features of both Type-A and Type-B, resulting in a central flat area with radius $c = a + b$.

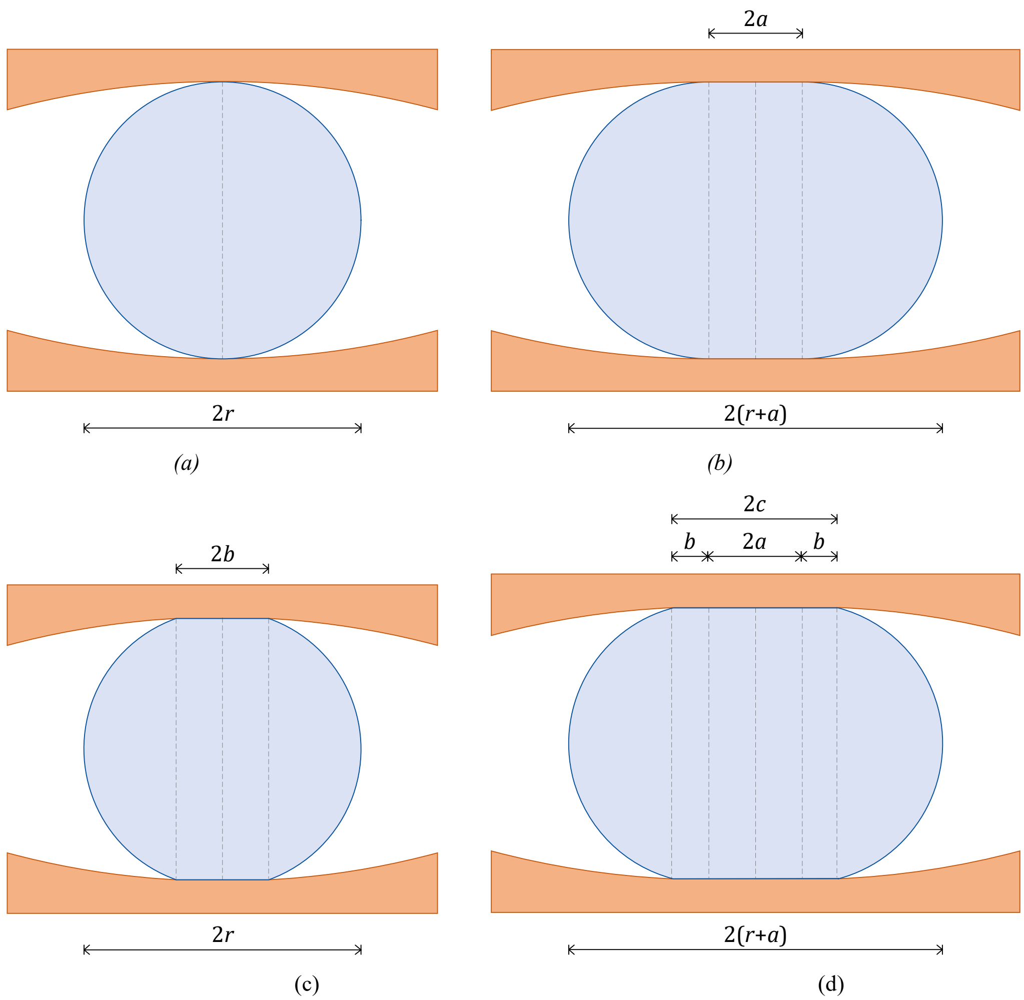

Figure 4. *Isolator types (a) Type-S (spherical, purely rolling isolator) (b) Type-A (rolling isolator with impact) (c) Type-B (rocking/rolling isolator with impact) (d) Type-C (rocking/rolling isolator with impact, a combination of Type-A and Type-B).*

TYPE-S ISOLATOR

It is insightful to analyze the behavior of the common spherical roller (type-S) before moving to the other types.

Kinematics

Figure 5a shows a 2D section of a spherical roller of radius r, rolling onto a flat surface. After the roller has rotated by θ, the center point C has moved to point C_3 and the contact point A_2 is directly below it, due to the flat horizontal rolling surface. However, when rolling occurs on a spherical surface of radius R_2 (Figure 5b), the contact point A_2 is further to the right, forming an angle θ_2 with the vertical axis. This angle is additional to the self-rotation angle θ. The difference between angles θ and $(\theta + \theta_2)$ is the root cause of the famous "coin paradox". Note that the angle θ_2 also indicates the rotation of the CG of the roller with respect to point C_2.

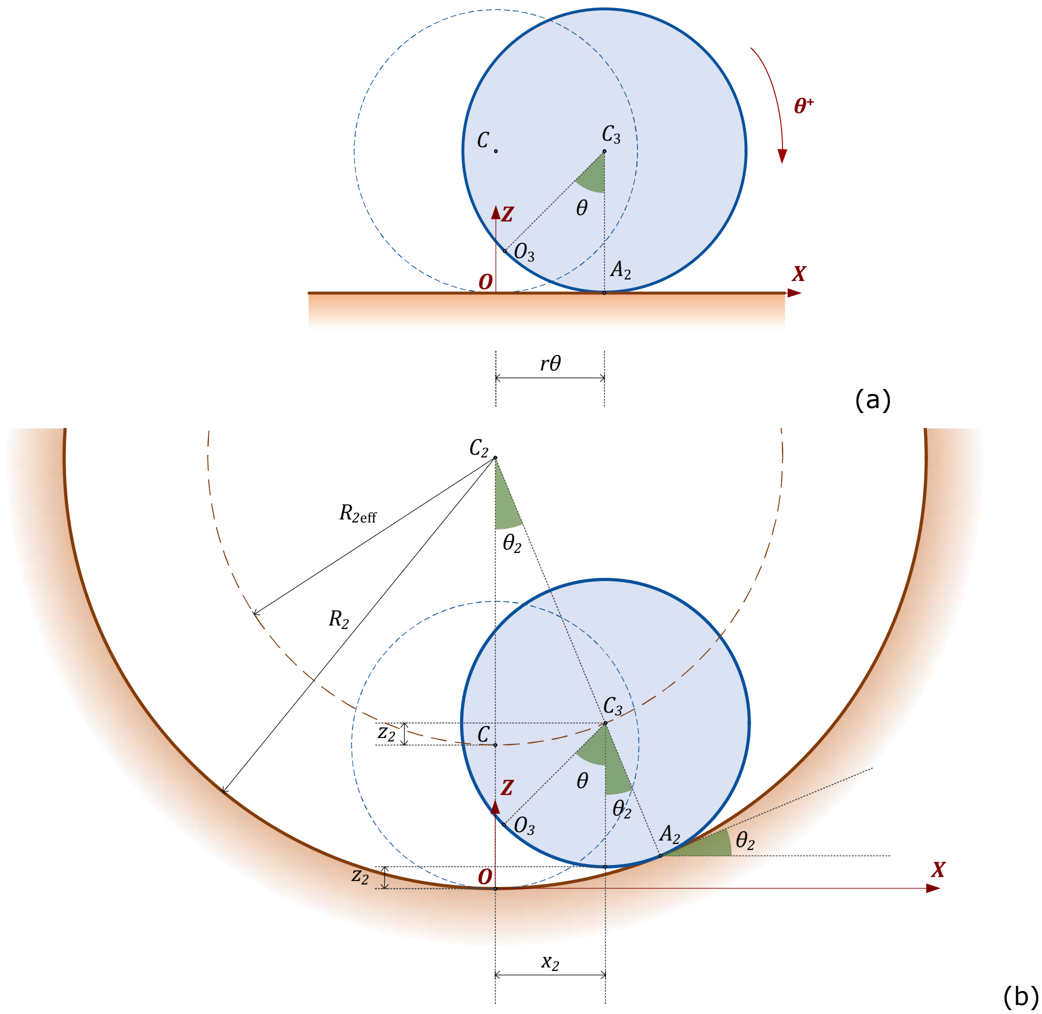

Figure 5. *Type-S isolator rolling on (a) flat surface and (b) spherical surface of radius* R_2

Since there is rolling without sliding, the arc length O_3A_2 must be equal to the arc length OA_2, which leads to

$$r(\theta + \theta_2) = R_2\theta_2 \tag{1}$$

By considering the effective radius $R_{2\text{eff}} = R_2 - r$ (Cilsalar & Constantinou, 2019), which is the radius of the circle on which the center of the roller is moving (Figure 5b), and by setting

$$\kappa_2 = \frac{r}{R_{2\text{eff}}} = \frac{r}{R_2 - r} \tag{2}$$

Equation (1) becomes

$$\theta_2 = \kappa_2\theta \tag{3}$$

Note that κ_2 is a measure of the relative curvature of the bottom base with respect to the roller radius r (Figure 6). When $\kappa_2 \to 0$, the bottom base is flat.

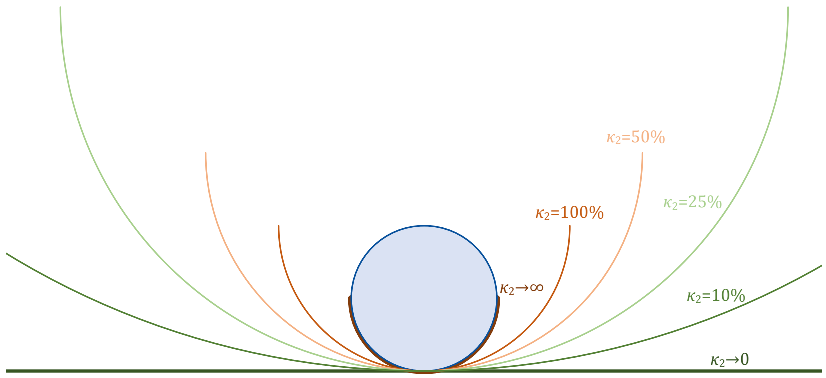

Figure 6. *Physical representation of curvature parameter κ_2.*

When concurrently rolling onto two surfaces of different radii (Figure 7), a curvature coefficient κ_1 needs to be defined in similar fashion.

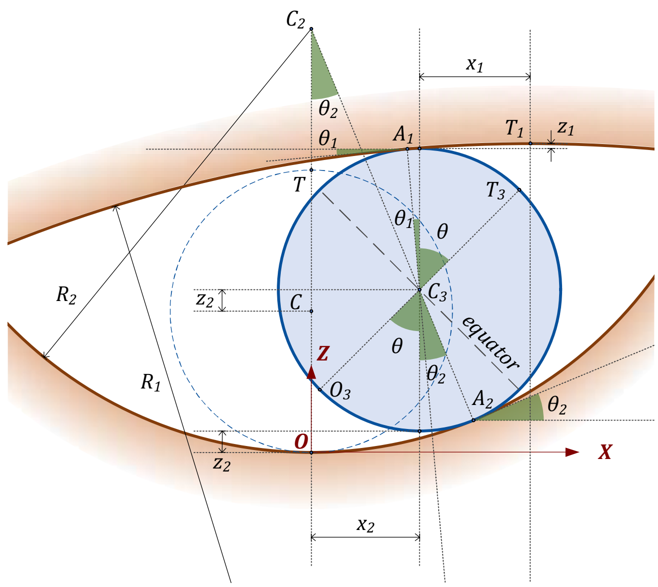

Figure 7. *2D section of a spherical roller rolling onto two spherical surfaces of different radii.*

The total horizontal displacement of the isolator (i.e., the horizontal distance of point T_1 with respect to the initial point T) is given as

$$x_b(\theta) = x_1 + x_2 = r\left(\frac{1}{\kappa_1}\sin(\kappa_1\theta) + \frac{1}{\kappa_2}\sin(\kappa_2\theta)\right) \tag{4}$$

The total vertical displacement (uplifting) of the isolator (i.e., the vertical distance of point T_1 with respect to point T) is given as

$$z_b(\theta) = z_1 + z_2 = r\left(\frac{1}{\kappa_1}(1-\cos(\kappa_1\theta)) + \frac{1}{\kappa_2}(1-\cos(\kappa_2\theta))\right) \quad (5)$$

Equations of motion

Following Wang (Wang, 2005), we perform a force analysis of the different bodies of the isolator, where M is the mass of the superstructure, m is the mass of the roller, I_3 is the moment of inertia of the roller about its CG, N_1 and N_2 are the normal forces at the points of contact, and F_{f1} and F_{f2} are the necessary frictional forces to maintain the non-slip condition (Figure 8).

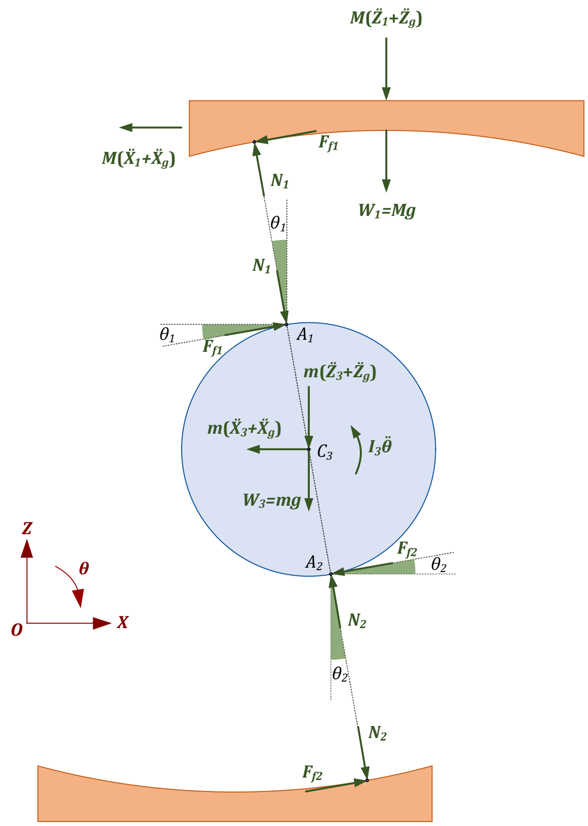

Figure 8. *Force analysis for the bodies of the Type-S isolator.*

The following set of equations can be derived:

$$(N_1\sin\theta_1 - N_2\sin\theta_2) + \mathrm{sign}(\dot{x}_b)\left(F_{f1}\cos\theta_1 - F_{f2}\cos\theta_2\right) - m\left(r\ddot{\theta}\cos\theta_2 + \ddot{X}_g\right) = 0 \quad (6)$$

$$-N_1\cos\theta_1 + N_2\cos\theta_2 + \mathrm{sign}(\dot{x}_b)\left(F_{f1}\sin\theta_1 - F_{f2}\sin\theta_2\right) - m\left(r\ddot{\theta}\sin\theta_2 + \ddot{Z}_g + g\right) = 0 \quad (7)$$

$$-I_3\ddot{\theta} + r\,\mathrm{sign}(\dot{x}_b)\left(F_{f1} + F_{f2}\right) = 0 \quad (8)$$

$$-N_1\sin\theta_1 - F_{f1}\cos\theta_1\,\mathrm{sign}(\dot{x}_b) - M\left(r\ddot{\theta}(\cos\theta_1 + \cos\theta_2) + \ddot{X}_g\right) = 0 \quad (9)$$

$$N_1\cos\theta_1 - F_{f1}\sin\theta_1\,\mathrm{sign}(\dot{x}_b) - M\left(r\ddot{\theta}(\sin\theta_1 + \sin\theta_2) + \ddot{Z}_g + g\right) = 0 \quad (10)$$

The system of five equations, i.e., Equations (6) to (10) is solved and after some simplifications and substitutions, the angular acceleration $\ddot{\theta}$ is found to be

$$\ddot{\theta} = -\frac{\left(g+\ddot{Z}_g\right)\left(\sin(\kappa_1\theta)+\left(1+\frac{m}{M}\right)\sin(\kappa_2\theta)\right)+\ddot{X}_g\left(\cos(\kappa_1\theta)+\left(1+\frac{m}{M}\right)\cos(\kappa_2\theta)\right)}{\frac{I_3}{rM}+\left(2+\frac{m}{M}+2\cos(\kappa_1\theta-\kappa_2\theta)\right)r} \quad (11)$$

Solving the previous equation numerically for $\theta = \theta(t)$ allows for the evaluation of any other quantity of interest, as well as simulating the motion of the isolator for validation purposes, as will be demonstrated.

Linearized equation of motion

We can linearize Equation (11) for small angles and obtain

$$\ddot{\theta} = -\frac{\left(g+\ddot{Z}_g\right)\left(\kappa_1+\left(1+\frac{m}{M}\right)\kappa_2\right)\theta+\ddot{X}_g\left(2+\frac{m}{M}\right)}{\frac{I_3}{rM}+\left(4+\frac{m}{M}\right)r} \quad (12)$$

Regarding the undamped free vibration, the previous equation becomes

$$\left(\frac{I_3}{rM}+\left(4+\frac{m}{M}\right)r\right)\ddot{\theta}+g\left(\kappa_1+\kappa_2\left(1+\frac{m}{M}\right)\right)\theta = 0 \quad (13)$$

From which the natural period of oscillation is evaluated as

$$T_n = 2\pi\sqrt{\frac{\frac{I_3}{rM}+\left(4+\frac{m}{M}\right)r}{g\left(\kappa_1+\kappa_2\left(1+\frac{m}{M}\right)\right)}} \quad (14)$$

If we further simplify the previous equation for $I_3 \ll rM$ and $m \ll M$, and assume that the curvature of the top and bottom plates are the same ($\kappa_1 = \kappa_2 = \kappa$), we obtain

$$T_n = 2\pi\sqrt{\frac{2r}{g\kappa}} \quad (15)$$

Which is equivalent to the corresponding equation of the double spherical sliding system since $R_{\text{eff}} = r/\kappa$. Solving the last equation for κ we derive

$$\kappa = \frac{8\pi^2 r}{gT_n^2} \quad (16)$$

Which yields the necessary parameter κ for a given target period of oscillation.

VISUAL SEISMIC SIMULATIONS

The previous equations of motion for the Type-S bearing have been coded in Mathematica (Wolfram Research, 2024) to visually simulate seismic events. The response of the bearing is displayed along with the ground movement and graphs of all relevant metrics to ensure that motion is natural and no significant error exists.

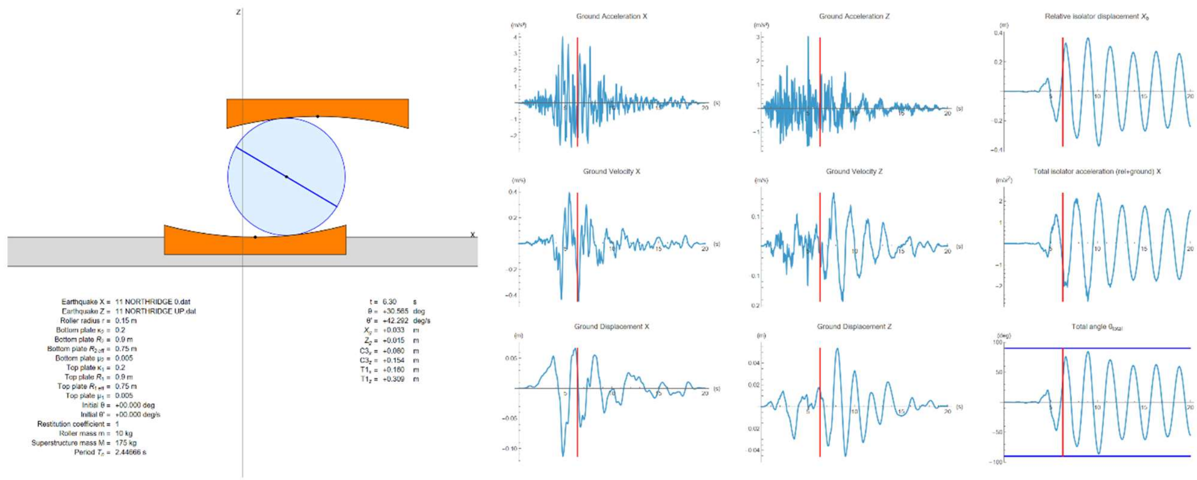

Figure 9. *Visual seismic simulations in Mathematica (Wolfram Research, 2024).*

SMALL-SCALE EXPERIMENTS

Preliminary small-scale experiments with 3D printed Type-B isolators in a small shake table confirm that the isolator behaves very satisfactorily. In particular, it is activated after a certain threshold, it prevents free-standing slender specimens from toppling and fully recenters at the end of the event. Interestingly, there also appears to be a significant level of damping due to the impacts and the interlocking motion of the gear teeth.

Figure 10. *Small scale experiments of Type-B isolators.*

Several free-standing wood specimens ($B = 120\ \mathrm{mm} \times D = 60\ \mathrm{mm}$) of various heights H were tested against strong seismic records. Small indentations on the top plate prevented sliding, although it is uncertain if they were necessary at all. Under unfavorable conditions (flexible top plate, unprepared wood surfaces, small depth D), specimens with $H/B = 6$ reliably remained intact after all available records, while in certain cases even specimens with $H/B = 10$ did not topple.

CONCLUSIONS

The 3DGRIPS system presents an advancement in the seismic isolation of lightweight, high-value assets, successfully addressing several limitations inherent in conventional isolation technologies. The system features a central flat area which provides stress alleviation and impact-related damping, while ensuring precise automatic recentering following a seismic event. Further, since the 3DGRIPS bearing is designed for minimal deformation, its kinematic equations can be formulated with high accuracy using geometric principles, bypassing the need for complex, computationally intensive modeling. This geometric precision, combined with the system's inherent non-sliding nature, ensures long-term reliability compared to traditional sliding isolators, which often require careful investigation into the temporal evolution of friction coefficients due to aging and environmental contamination. Preliminary small-scale experiments, conducted with 3D-printed prototypes on a shake table, have confirmed the system's effectiveness; tested specimens remained upright after several strong seismic records, demonstrating the bearing's reliability. In total, the 3DGRIPS system offers a robust, advantageous solution that ensures both enhanced resilience and operational continuity for high-value protection applications.

3DGRIPS is an ongoing project. More up-to-date information can be found at https://3dgrips.eu.

ACKNOWLEDGEMENTS

The research project titled “Three-dimensional seismic isolation of sensitive artefacts and equipment by Geared Rocking/Rolling Inverse Pendulum System – 3DGRIPS” is implemented in the framework of H.F.R.I call “3rd Call for H.F.R.I.’s Research Projects to Support Faculty Members & Researchers” (H.F.R.I. Project Number: 23284).

REFERENCES

Charalampakis, A. (2023). *Geared rocking/rolling inverse pendulum system for the three–dimensional seismic isolation of structures and infrastructure.* (Patent Hellenic Industrial Property Organisation (OBI) Patent No. 1010370). Hellenic Industrial Property Organisation. https://www.obi.gr/wp-content/uploads/2023/02/EDBI_A_2023_01.pdf

Cilsalar, H., & Constantinou, M. C. (2019). Behavior of a spherical deformable rolling seismic isolator for lightweight residential construction. *Bulletin of Earthquake Engineering*, *17*(7), 4321–4345. https://doi.org/10.1007/S10518-019-00626-Z/TABLES/7

Giarlelis, C., Keen, J., Lamprinou, E., Martin, V., & Poulios, G. (2018). The seismic isolated Stavros Niarchos Foundation Cultural Center in Athens (SNFCC). *Soil Dynamics and Earthquake Engineering*, *114*, 534–547. https://doi.org/10.1016/J.SOILDYN.2018.05.011

Koumousis V.K. (2008). Seismic isolation system for the statue of Hermes at the archaeological museum of Olympia. *Advances in the Protection of Museum Collections from Earthquake Damage*, 125–134.

Touaillon, J. (1870). *Improvement in buildings* (Patent US99973A). https://patents.google.com/patent/US99973A/en

Wang, J. (2005). *Seismic isolation analysis of a roller isolation system* [PhD Thesis]. State University of New York at Buffalo.

Wolfram Research, Inc. (2024). *Mathematica* (14.1). Wolfram Research, Inc. https://www.wolfram.com/mathematica